AUTOMATED FORWARD MECHANICAL MODELING OF WRINKLE RIDGES ON MARS. Amanda L. Nahm[1] and Samuel H. Peterson[2], [1]Institut für Planetenforschung, German Aerospace Center (DLR), Rutherfordst. 2, 12489 Berlin, Germany, amanda.nahm@dlr.de, [2]Schleiermacherst. 12, 10961 Berlin, Germany, sam.houston.peterson@gmail.com.

Introduction: The InSight (Interior Exploration using Seismic Investigations, Geodesy and Heat Transport) mission to Mars, was scheduled to launch in March 2016, but has been recently postponed. One of the main goals of the mission is to understand the internal structure of Mars [1], in part through passive seismology (the SEIS instrument [2]). Understanding the shallow surface structure of the landing site is critical to the robust interpretation of recorded seismic signals.

The proposed InSight landing ellipses are located in western Elysium Planitia on primarily Hesperian and Amazonian aged lava flows [3, 4]. Faults, such as the wrinkle ridges abundant in this area, can be used to determine the subsurface structure of the regions they deform. For example, wrinkle ridges have been used to probe the subsurface mechanical structure elsewhere on Mars [e.g., 5, 6]. Here, we test a new automated method for forward mechanical modeling of the topography of a wrinkle ridge in Elysium Planitia. This method will allow for faster and more robust determination of subsurface fault geometry, allowing interpretation of the subsurface structure in the area.

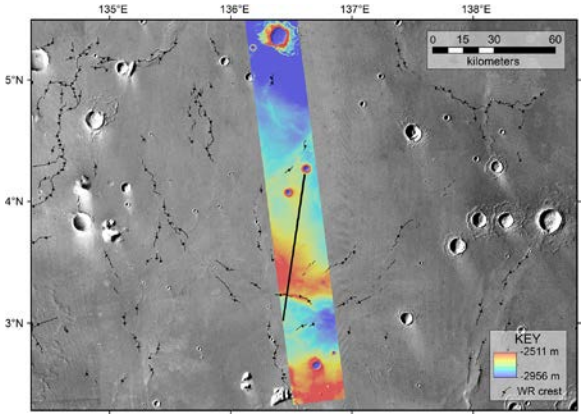

Figure 1. CTX DTM with High Resolution Stereo Camera (HRSC) base map for context. Profile location shown by heavy black line on DTM. WR mapped by J. Voigt.

Approach: *Forward mechanical modeling:* We adopt the standard technique of forward mechanical modeling of fault-related topography [*e.g.*, 7, 8]. We use the forward mechanical dislocation modeling program Coulomb* [9, 10] to model displacements of the surface induced by blind thrust faulting. Stress and material displacement calculations are made in an elastic half-space with uniform isotropic properties following the equations derived by [11]. In these models, a fault is idealized as a rectangular plane with a specified sense of slip, magnitude of average displacement, fault dip angle, depths of the upper and lower fault tips, and fault length. Fault lengths are difficult to determine for WR, as they are typically not segmented and form complex, seemingly continuous structures. Here, we assume a fault length of 30 km (~the width of the CTX DTM), but also test the effects of different fault lengths on model results (see below). At present, we model the wrinkle ridge as a single blind thrust fault with a constant fault dip, acknowledging that WR are likely to have more complicated fault geometry [e.g., 5, 6, 12].

Typically, the modeling is performed using the Coulomb graphic user interface (GUI). This approach can be time consuming, requiring user inputs to change model parameters and to calculate the associated displacements for each model. This limits the number of models and the corresponding parameter space that can be tested. To reduce active user computation time and allow for a larger parameter space, we have developed a method in which the GUI is bypassed, but still uses the Coulomb software package. The general modeling procedure remains unchanged, though instead of the user iteratively varying the input parameters based on the model output, a set of input files are generated before modeling with ranges of pre-defined parameter values.

The calculations are divided into two suites. For Suite 1, a total of 3770 input files were generated in which the fault displacement (D), dip angle (δ), depth to upper fault tip (t), and depth to lower fault tip (B) were varied (Table 1). A second set of input files was created (Suite 2) after the best-fit model was determined (see below). Fault parameters were again varied, but with smaller range and incremental changes (Table 1), resulting in a total of 28,080 input files.

Table 1. Ranges for parameter values and incremental changes for Suites 1 and 2.

Suite	Parameter	Range	Increment
1	Displacement (m)	10-510	20
	Dip angle (°)	25-45	5
	Top (km)	1, 5, 10, 15	–
	Bottom (km)	5-40	5
2	Displacement (m)	110-250	10
	Dip angle (°)	20-45	1
	Top (km)	8-15	1
	Bottom (km)	25-39	2

RMS misfit calculations: The goodness of fit of the model to the data was determined using the Root Mean Square (RMS) metric. Mathematically, the

topographic data are represented as a function relating the distance along the WR profile to the displacement at that point, given by:

$$T(x_i),\ 0 \le x_i \le 80,\ i = 1,2,\dots,n \quad (1)$$

where T is the displacement (in m), x_i is the distance along the profile (in km), and n is the number of data points. The model calculated with Coulomb was defined on 1 km intervals along the profile. In order to compare the model to the topography values that fell between the model points, the model data were linearly interpolated. Let $\tilde{T}$ be the interpolated model:

$$\tilde{T}(x) = \tilde{T}(\underline{x})(1-\delta x) + \tilde{T}(\overline{x})(\delta x),\ 0 \le x \le 80 \quad (2)$$

where $\underline{x}$ denotes the largest integer less than x, $\overline{x}$ represents the smallest integer greater than x, and $\delta x = x - \underline{x}$. Note that for integer values, $\tilde{T}$ is given as the output of the Coulomb program. The RMS misfit (in m) is then calculated using the following equation:

$$RMS_{\tilde{T}} = \sqrt{\frac{1}{n}\sum_{i=1}^{i=n}\left(T(x_i) - \tilde{T}(x_i)\right)^2} \quad (3)$$

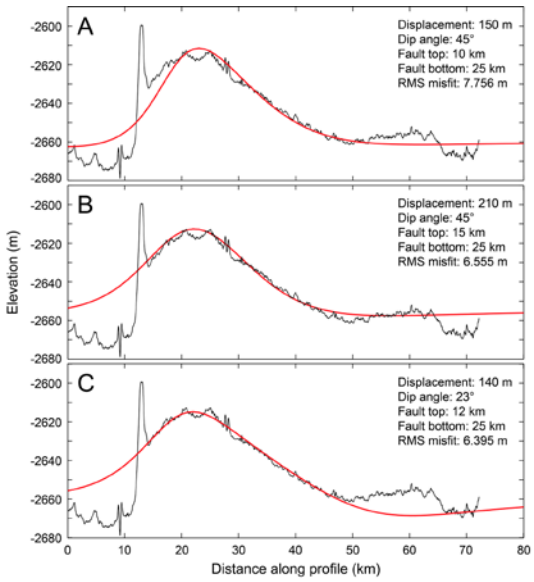

Figure 2. Results from different RMS misfit trials. Black line is average topographic profile and red line is model given by best fit parameters, shown in each panel. Fault length = 30 km. ~S to the left. A) Model with lowest RMS misfit determined over all x values; B) Model with lowest RMS misfit value for restricted x values (x = 11 to 50 km); C) Model with lowest RMS misfit for restricted x values (as in B) and smaller increments for a restricted parameter range (for details see text).

Results: RMS values were calculated for each Coulomb model. Models with the lowest RMS misfit values are taken to be the best-fit models. The best fit models, their parameter values, and RMS misfits are shown in Figure 2. Figure 2A shows the best fit model with RMS calculated over the entire x range (distance along profile). However, the thrust fault topography is only present between x = 11 and 50 km, so a second set of RMS calculations was performed with a restricted x range (Fig. 2B), reducing the RMS misfit by 1.2 m. Parameter ranges from models with RMS values 1 m larger than the minimum RMS value were used to define a narrower parameter space (Table 1, Suite 2). Displacements were calculated in Coulomb and the RMS values of the resulting models were determined. Fig. 2C shows the best fit model of this suite. The RMS value decreases again by 0.2 m, resulting in an overall reduction of the RMS value of ~1.4 m (18%).

Table 2. Effect of fault length on best-fit parameters and RMS misfit values, determined between x = 11 and 50 km. Parameter values are from Suite 1 (Table 1).

	15 km	**30 km**	**60 km**
Displacement (m)	410	210	190
Dip angle (°)	40	45	40
Top (km)	15	15	15
Bottom (km)	25	25	25
RMS misfit (m)	6.500	6.555	6.574

Table 2 shows the effect of fault length variations on best fit model parameters. Visually, the models are indistinguishable and thus are not shown here. Values for δ, t, B, and RMS misfit are either the same or very similar for each best fit model. The largest difference is observed in the displacement values. This discrepancy results from a linear relationship between fault displacement and length [e.g., 13], so to produce the same surface signal, fault displacement must necessarily be increased for shorter faults. These results indicate, however, that the subsurface structure (based on δ, t, and B) can be reliably determined from forward mechanical modeling even with uncertainty in fault length. Future work will test this method with the more realistic WR fault geometry.

References: [1] Banerdt et al. (2013), 44th LPSC, #1915. [2] Mimoun et al. (2012), 43rd LPSC, #1493. [3] Golombek et al. (2013), 44th LPSC, #1691. [4] Tanaka et al. (2014), PSS, 95, 11-24. [5] Watters (2004), Icarus, 171, 284-294. [6] Okubo and Schultz (2004), GSAB, 116, 597-605. [7] Cohen (1999), Adv. Geophys., 41, 133-231. [8] Schultz and Lin (2001), JGR, 106, 16549-16566. [9] Lin and Stein (2004), JGR, 109, B02303, doi:10.1029/2003JB002607. [10] Toda et al. (2005), JGR, 103, 24543-24565. [11] Okada (1992), Bull. Seismol. Soc. Am., 82, 1018-1040. [12] Schultz (2000), JGR, 105, 12035-12052. [13] Cowie and Scholz (1992), J. Struct. Geol., 14, 1149-1156.

*available from http://earthquake.usgs.gov/research/software/coulomb/

Acknowledgements: ALN is funded by an Alexander von Humboldt Foundation/Stiftung research fellowship. The authors thank I. Daubar (JPL) for the CTX DTMs used in this study.